micro

MDPI

Article

Micro 3D Printing by Two-Photon Polymerization: Configurations and Parameters for the Nanoscribe System

Ada-Ioana Bunea *, Nuria del Castillo Iniesta, Ariadni Droumpali, Alexandre Emmanuel Wetzel, Einstom Engay and Rafael Taboryski

National Centre for Nano Fabrication and Characterization (DTU Nanolab), Technical University of Denmark, Ørsted Plads 347, 2800 Lyngby, Denmark; nurin@dtu.dk (N.d.C.I.); adro@dtu.dk (A.D.); awet@dtu.dk (A.E.W.); einen@dtu.dk (E.E.); rata@dtu.dk (R.T.)

* Correspondence: adabu@dtu.dk

Abstract: 3D printing by two-photon polymerization enables the fabrication of microstructures with complex shapes and critical dimensions of a few hundreds of nanometers. On state-of-the art commercial two-photon polymerization systems, an immense 3D design freedom can be put into practice by direct laser writing using a precise fabrication technology, which makes this approach highly attractive for different applications on the microscale, such as microrobotics, micro-optics, or biosensing. However, navigating the different possible configurations and selecting the optimal parameters for the fabrication process often requires intensive testing and optimization. In addition to the more established acrylate-based resins, there is a growing interest in the use of soft materials. In this paper, we demonstrate the fabrication of various microscale structures by two-photon polymerization using a Nanoscribe Photonic Professional GT+ commercial system. Furthermore, we describe the different configurations of the system and parameter selection, as well as commercial resins and their chemical and mechanical properties. Finally, we provide a short guide aiming to serve as starting point for the two-photon polymerization-based fabrication of various microscale architectures with distinct characteristics.

Keywords: 3D printing; two-photon polymerization; direct laser writing; microfabrication; surface chemistry

Citation: Bunea, A.-I.; del Castillo Iniesta, N.; Droumpali, A.; Wetzel, A.E.; Engay, E.; Taboryski, R. Micro 3D Printing by Two-Photon Polymerization: Configurations and Parameters for the Nanoscribe System. *Micro* **2021**, *1*, 164–180. https://doi.org/10.3390/micro1020013

Academic Editor: Keekyoung Kim

Received: 30 July 2021
Accepted: 16 September 2021
Published: 25 September 2021

1. Introduction

3D printing, also known as rapid prototyping or additive manufacturing, has become one of the world's greatest tools for small-scale manufacturing and is increasingly used for large-scale production. Pioneered in the late 1980s [1], 3D printing has been developing at an incredible pace in recent years and has proven useful for, e.g., medical applications [2], the constructions industry [3], or even preparing food [4]. A plethora of 3D printing equipment for various size scales is already commercially available, while further technological developments in the field are being explored in many research laboratories around the world.

Among the different approaches to 3D printing, two-photon polymerization (2PP) enables the highest spatial resolution, with features smaller than Abbe's diffraction limit being produced due to non-linear light-induced effects in the photoresponsive material [5,6]. 2PP relies on two-photon excitation, a phenomenon first described by Göppert-Mayer in 1931 [7] and demonstrated experimentally in 1961 [8], soon after the invention of pulsed lasers. Micro 3D printing by 2PP [9,10] was pioneered in the late '90s [11] and has since found applications in, e.g., microrobotics [12,13], biosensing [14,15], biomedical research [16,17], optical data storage [18], micro-optics [19,20], antireflective surfaces [21], photonic metamaterials [22], photonic crystals [23], or mechanical metamaterials [24].

In its early stages, 2PP 3D printing was only available using home-made setups. However, less than a decade after 2PP 3D printing was first demonstrated, commercial

equipment became available and the field naturally started to grow. Nanoscribe, founded in 2007, was the first company to commercialize 2PP DLW systems. Other noteworthy 2PP equipment providers that have emerged since are Microlight3D, Multiphoton Optics, UpNano, and Femtika. Typically, the light employed for the 2PP process comes from a pulsed laser with a repetition rate in the order of tens of MHz, and the systems use green light (515 nm or 532 nm), near-infrared light (~780 nm, 1064 nm, or 1080 nm), or a combination of these wavelengths. 3D printing by 2PP is a direct laser writing (DLW) technique in which the solid structure is written into a liquid resin voxel-by-voxel, by scanning a femtosecond-pulsed tightly focused laser beam (Figure 1). Most commercial resins suitable for 2PP are based on acrylate or epoxy chemistry. In-house mixtures are also common, particularly for printing stimuli-responsive structures [25–27]. Recently, given the fact that 2PP systems are becoming more widespread, the interest for comparing various 2PP systems and their dimensional accuracy has grown [28].

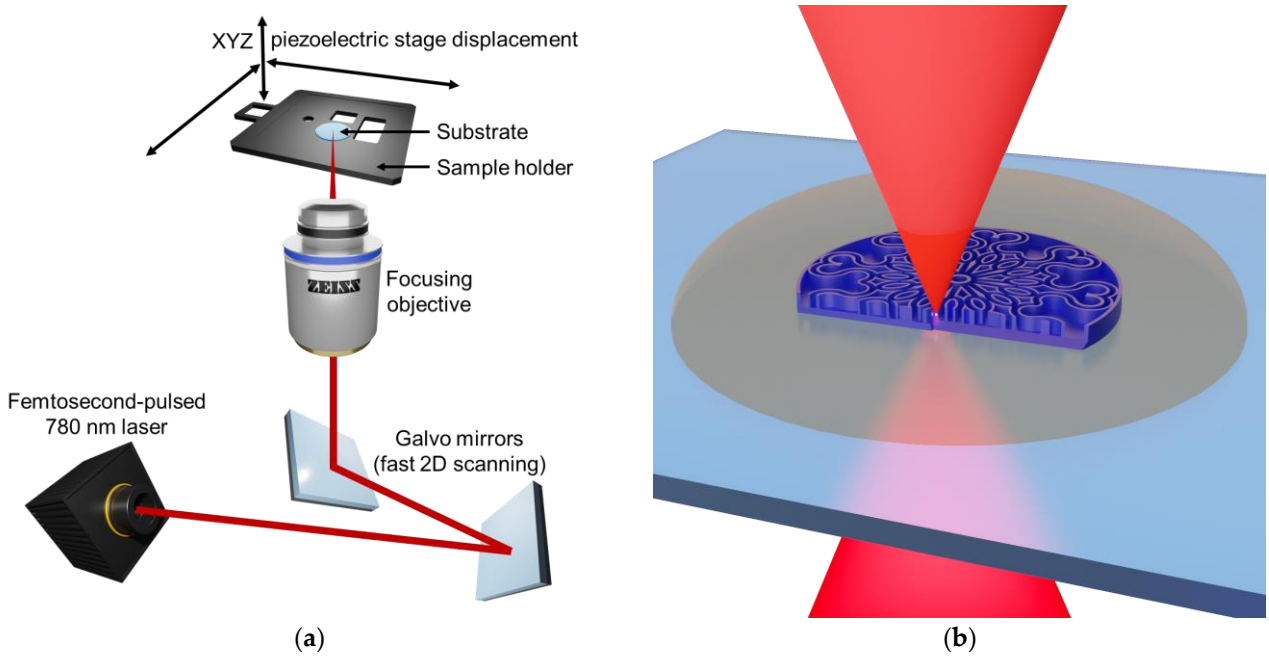

Figure 1. Schematic representation of two-photon polymerization direct laser writing. (**a**) The beam coming from a femtosecond-pulsed laser is scanned in 2D using a high-speed galvo mirror system and subsequently focused into the sample through a microscope objective. The stage on which the sample is located can also be displaced in X, Y, or Z by a piezo system. (**b**) By scanning the laser focal point, the target structure is written into the liquid resin voxel-by-voxel.

Our lab was among the first in the world to acquire Nanoscribe Photonic Professional equipment. This system enabled precise microfabrication, but did not include a galvo mirror scanning system. Instead, beam scanning was achieved solely by displacing the sample stage in XYZ using the piezo motors, which made it extremely slow. Recently, we upgraded to the Nanoscribe Photonic Professional GT+ system (equivalent to the GT2 system), which includes the galvo mirrors scanning system and enables much faster 3D microfabrication. Due to the reduced fabrication time, we have been able to expand our microfabrication portfolio in terms of structure size, shape, and material.

The commercial 2PP system is extremely versatile. However, in our experience, navigating its different possible configurations and selecting the optimal parameters for a specific structure often requires intensive testing and optimization. Nanoscribe provides a test file for rapid screening of the laser power and scan speed on individual systems. Using this typically represents the first optimization step when switching to a new configuration, a new resin, or simply for periodically checking the printer's behavior. The influence of laser power and scan speed on the properties of 3D printed structures was also discussed

by several groups [29–31], whereas voxel optimization was recently described elsewhere for an in-house 2PP resin [32]. The laser power and scan speed have indeed a critical influence on the quality of the printing, which is why most users of a 2PP printer will likely investigate these parameters. However, the optimal laser power and scan speed depend more on the fabrication system than on the structure itself, so it is often sufficient to optimize them on the standard test structures for every configuration of the system, and to perform further optimization steps only for highly demanding samples with, e.g., features close to the resolution limit. On the other hand, other parameters of the 2PP DLW process are often overlooked in the optimization process, as they are more circumstantial, and depend on each structure's parameters, such as total size, minimum feature size, mechanical parameters, or aspect ratio.

In addition to optimizing the fabrication parameters, various post-processing strategies can be employed to confer the desired properties for 2PP 3D printed structures. For example, additional curing of the polymer after the DLW process was shown to increase the degree of crosslinking [29,33]. An improved development procedure including additional UV curing fostered the fabrication of pillar arrays [34]. Isotropic plasma etching and/or pyrolysis were used to further improve the resolution and achieve critical dimensions below 100 nm [35], while thermal reflow was shown to improve the surface smoothness of microstructures [36,37]. While these options are extremely valuable for pushing the limits of the 2PP technology, they are not meant to replace structure optimization, but instead benefit from having a good quality print for further processing.

In this paper, we showcase five distinct types of microscale structures fabricated by 2PP DLW. The microscale structures are written using different configurations of our Nanoscribe system, three different microscope objectives, and three different commercial resins. We provide a short guide on initial parameter selection, which aims to serve as starting point for the 2PP fabrication of microscale architectures with different characteristics, as well as a detailed list of all the parameters employed for the fabrication of the structures presented herein. To the best of our knowledge, such a comparison of different printing configurations is not available in the literature, and it should prove highly beneficial for less experienced Nanoscribe users, and potentially also for users of other two-photon polymerization systems.

In addition to the "quick start" guide, we also suggest potential uses for the different microscale architecture types presented herein as examples. This is meant to inspire newcomers to the field to experiment with microscale 3D printing, as well as to help reduce the optimization time for producing high quality structures.

2. Materials and Methods

2.1. Fabrication by Two-Photon Polymerization Direct Laser Writing

The 3D design .STL files were imported into the DeScribe software, version 2.5.5 (Nanoscribe, Karlsruhe, Germany). 3D renders of all of the 3D designs are shown in Section S1 of the Supplementary Materials, together with details about the sizes of the designed structures. The fabrication parameters were set as described in Section S2 of the Supplementary Materials, in order to generate the .GWL job file. Fabrication was then performed by direct laser writing (DLW) using two-photon polymerization (2PP) on a Nanoscribe Photonic Professional GT+ system (Nanoscribe, Karlsruhe, Germany). The system employs a femtosecond fiber laser source with a wavelength centered at 780 nm, a laser power ranging between 50 mW and 150 mW, a pulse length between 100 fs and 200 fs, and a repetition rate of 80 MHz.

Three different microscope objectives were used to focus the laser light into the sample, as specified for individual structures: (1) Plan-APOCHROMAT 63×/1.40 Oil DIC objective (Carl Zeiss, Oberkochen, Germany); (2) LCI Plan-Neofluar 25×/0.8 Imm Corr DIC M27 for water, silicone oil, glycerine, or oil immersion (Carl Zeiss, Oberkochen, Germany); (3) EC Epiplan-Neofluar 20×/0.50 DIC M27 (Carl Zeiss, Oberkochen, Germany). In the main text,

we refer to the microscope objectives simply by stating the magnification and numerical aperture, i.e., 63×/1.40, 25×/0.8, or 20×/0.50.

Three different types of substrates were used, as specified for individual structures: (1) 170 µm thick borosilicate glass coverslips; (2) 0.7 mm thick 30 × 30 mm^2 fused silica; and (3) 0.7 mm thick 30 × 30 mm^2 glass coated with indium-tin oxide (ITO) on one side. Prior to printing, all the substrates were cleaned by rinsing with ethanol and deionized water, and subsequently blow-dried with air. The ITO-coated substrates were activated prior to use by 75 s oxygen plasma treatment using a Zepto low pressure plasma system (Diener, Ebhausen, Germany).

Three different resins were used, as specified for individual structures: (1) IP-PDMS; (2) IP-L 780; and (3) IP-Dip. After printing, uncrosslinked IP-PDMS and IP-L 780 were removed by 20 min incubation in isopropanol, whereas uncrosslinked IP-Dip was removed by 20 min incubation in propylene glycol monomethyl ether acetate (PGMEA), followed by 5 min incubation in isopropanol. After development, all structures were allowed to dry horizontally at room temperature before characterization. The fabrication process was conducted entirely at room temperature.

For each type of structure, the fabrication parameters were optimized in an iterative process. Subsequently, the structures with optimized parameters were printed in triplicate, and imaged using scanning electron microscopy (SEM).

2.2. Structure Characterization by Scanning Electron Microscopy

SEM imaging of all the samples was performed using a Zeiss Supra 40 VP (Carl Zeiss, Oberkochen, Germany) scanning electron microscope. Prior to SEM imaging, the samples were coated with a thin gold layer (15–30 nm) using a sputter coater (Cressington Scientific Instruments, Watford, UK). All images were acquired in high vacuum mode using an acceleration voltage of 1.0 to 1.5 kV and the secondary electron detector. The triplicate structures were imaged, and representative images were selected for the Results section.

2.3. Structure Characterization by Optical Profilometry

A 3D optical profiler confocal interference microscope (S Neox 3D Optical Profiler, Terrassa, Spain) equipped with a 50×/0.80 objective was used to investigate the height profile of the fabricated structures. With the 50×/0.80 objective, the field of view is 337.82 µm × 282.62 µm, and the pixel resolution limit is 0.51 µm. The acquisition of the 3D profile was carried out using a basic confocal mode, with a relative piezo Z scanning, an average of 3 images and a speed factor of 1× for higher resolution. Gwyddion, a free data analysis software for scanning probe microscopy was used for the analysis of the acquired 3D profiles [38]. For the reconstruction of the 3D images, simple plane leveling was performed to shift the background surface to zero.

2.4. Structure Characterization by X-ray Photoelectron Spectroscopy

X-ray photoelectron spectroscopy (XPS) was performed on flat structures prepared using the three different resins, i.e., IP-PDMS, IP-L 780, IP-Dip, and IP-PDMS, using the Nexsa X-ray Photoelectron Spectrometer System (ThermoFisher Scientific Inc., Waltham, MA, USA). The XPS analysis was performed using monochromated Al-Kα radiation at 1486.6 eV, with a spot size of 100 µm, and a flood gun for charge compensation. For each sample, XPS data included a survey spectrum, acquired by averaging 4 scanned measurements, and high-resolution spectra for C, O, and Si, acquired by averaging 10 scanned measurements. Data acquisition and analysis was performed using the Avantage software V5.9925 (ThermoFisher Scientific Inc., Waltham, MA, USA).

3. Results

In order to emphasize the flexibility of the 2PP 3D printing technology, we have chosen five types of microstructures with distinct characteristics. Two soft microstructures were fabricated using a resin recently released by Nanoscribe: a soft mold, and a porous scaffold.

Two high-resolution structures were printed using acrylic resins: a flat structure which can be considered 2.5D, and a truly 3D architecture. We also demonstrate the fabrication of a macroscopic structure using an acrylic resin. Table 1 shows a "quick start" guide for printing structures with such different characteristics.

Table 1. Quick start guide for selecting the microscope objective, configuration, substrate, IP-series resin, slicing, and hatching distances on the Nanoscribe, depending on the type of target microstructure.

Type of Structure	Microscope Objective	Configuration	Substrate	Resin	Slicing‖Hatching Distance (nm)	
Soft	25×/0.80	DiLL	Activated ITO-coated glass	IP-PDMS	300	300
High resolution, flat	63×/1.40	(Oil) Immersion	170 µm thick borosilicate glass	IP-L 780	300	200
High resolution, tall	63×/1.40	DiLL	Fused silica	IP-Dip	300	200
Large	20×/0.50	(Air) Immersion	170 µm thick borosilicate glass	IP-L 780 *	500	500

* Nanoscribe recommends the use of AZ resists for the 20×/0.50 objective.

All structures shown in this paper were printed using the following parameters: *GalvoScanMode*, *ContinuousMode*, voxel aspect ratio 3.5, stage velocity 200 µm·s^{-1}, Base count 0, and Hatching angle 90°. The other fabrication parameters employed for producing the structures are compiled in Table 2.

Table 2. Fabrication parameters employed for the different 3D printed structures.

	Soft Structures		Mandala		Sphynx & Pyramid		Yggdrasil	
	Mold	Porous	"Good"	"Bad"	"Good"	"Bad"	"Good"	"Bad"
Microscope objective	25×/0.80		63×/1.40		63×/1.40		20×/0.50	63×/1.40
Configuration	DiLL		Oil immersion	DiLL	DiLL	Oil immersion	(Air) Immersion	Oil immersion
Substrate	Activated ITO-coated glass		170 µm thick borosilicate glass	Fused silica	Fused silica	170 µm thick borosilicate glass	170 µm thick borosilicate glass	
Resin	IP-PDMS		IP-L 780	IP-Dip	IP-Dip	IP-L 780	IP-L 780	
Slicing mode	Fixed		Fixed		Fixed		Fixed	
Slicing distance (µm)	0.3		0.2		0.3		0.5	0.3
Contour count	2	1	0		2		3	
Hatching distance (µm)	0.2	0.3	0.2		0.3		0.5	0.2
Laser power (%)	50	75	50		50		60	50
Scan speed (µm·s^{-1})	10,000	20,000	10,000		10,000		500	10,000

The information compiled in Table 1 is not provided as such in the Introduction guide received from Nanoscribe after the equipment's installation, which is why we chose to compile this "quick start" guide based on our experience with the printer. Furthermore, we highlight a few aspects, as compared to the producer's recommendations. Firstly, the recommended slicing and hatching distances of 200–400 nm for IP-PDMS printing were found reasonable in our experiments, as we found that using 300 nm for both slicing and hatching was optimal. Secondly, the company suggests a slicing distance of 500 nm for the 63×/1.40 objective, whereas our optimized structures were obtained using a slicing distance of 300 nm. However, the reduced slicing distance implies an increased printing time, so this trade-off should be considered based on individual needs. The company's suggested hatching distance of 200 nm for the 63×/1.40 objective was deemed optimal in our experiments. Finally, Nanoscribe recommends the use of AZ resists for the 20×/0.50 objective.

Nevertheless, we demonstrated successful printing of a large structure using the 20×/0.50, the IP-L 780 resin, slicing and hatching distances of 500 nm, a laser power of 60%, and a very slow scan speed of 500 µm·s^{-1}. We do not consider this objective/resin combination optimal, but we chose to include this recipe in the "quick start" guide as an option for using an IP-series resin together with the 20×/0.50 objective, and still obtaining a good quality print.

3.1. Soft Structures

Given the growing interest in the 2PP DLW of soft materials, Nanoscribe recently released the resin IP-PDMS, which enables the fabrication of structures with properties similar to polydimethylsiloxane (PDMS). Here, we report the beta test of this new resin, IP-PDMS, in what is, to the best of our knowledge, the first use of this recently developed resin in a scientific publication.

Microscale replication is often made with molds made from hard materials, such as electroformed Ni [39,40], but may also be formed using soft resins [41,42]. Therefore, 3D printing of soft structures could be very valuable for producing master molds that can be used for subsequent replication. We chose a rosette window cookie pattern (Figure 2) to demonstrate the ability of 2PP to fabricate a soft master mold suitable for subsequent replication. From the optical profiler recordings, the total measured height of the cookie mold is 18 µm, and the height of the mold's walls is 9 µm. These values are in good agreement with the design, where the total height of the cookie mold was set to 17 µm, and the height of the mold's walls to 11 µm.

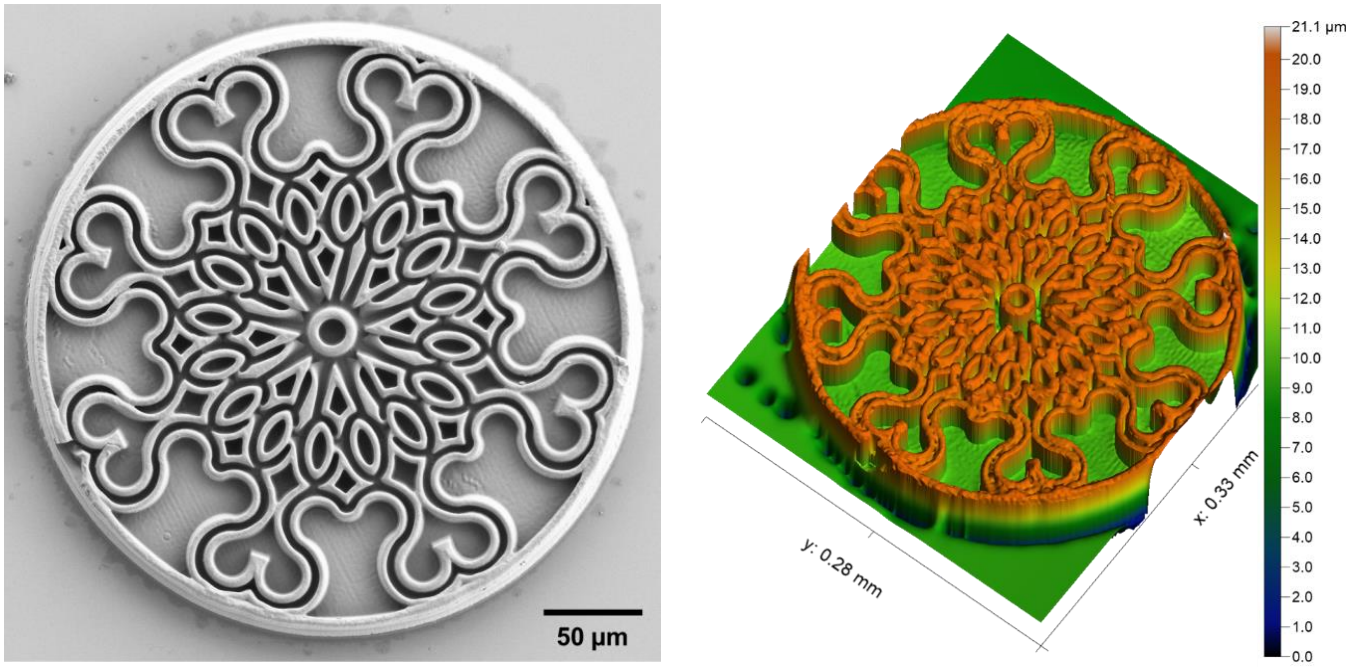

(**a**) (**b**)

Figure 2. Rosette window cookie master mold structure. The entire structure has a diameter of 300 µm, a total thickness of 18 µm, and its walls are 9 µm tall. The structure was printed in the IP-PDMS resin on a plasma treated ITO-coated fused silica substrate using the 25×/0.80 microscope objective. (**a**) Scanning electron micrograph. (**b**) Natural proportion image generated using optical profilometry.

Soft microscale architectures are also extremely interesting for biomedical applications. We recently reported the use of 3D printed polymeric scaffolds as biomimetic cell membrane supports [16]. However, the scaffolds in that study were fabricated using the IP-L 780 resin, which means that they had a Young's modulus > 2 GPa [43], significantly higher than that of the corresponding structures encountered in nature. The IP-PDMS

resin is more than 100 times softer, with a Young's modulus of 15.3 MPa, according to the producer's specifications. This elastic modulus value is similar to that of human connective tissues, specifically ligaments and cartilage [44]. Therefore, we decided to fabricate a soft porous structure with an arbitrary geometry, mimicking to some extent the structure of the connective tissues encountered in the human body (Figure 3). The porous scaffold is a cube with a side length of 133 µm. Despite the relatively soft nature of the polymer, the porous scaffold was stable during chemical development and subsequent functionalization, including exposure to high vacuum conditions and gold sputtering. The porosity of the structure was investigated using SEM, which confirmed that the network of pores penetrates beyond the outermost surface of the structure, into its bulk (data not shown).

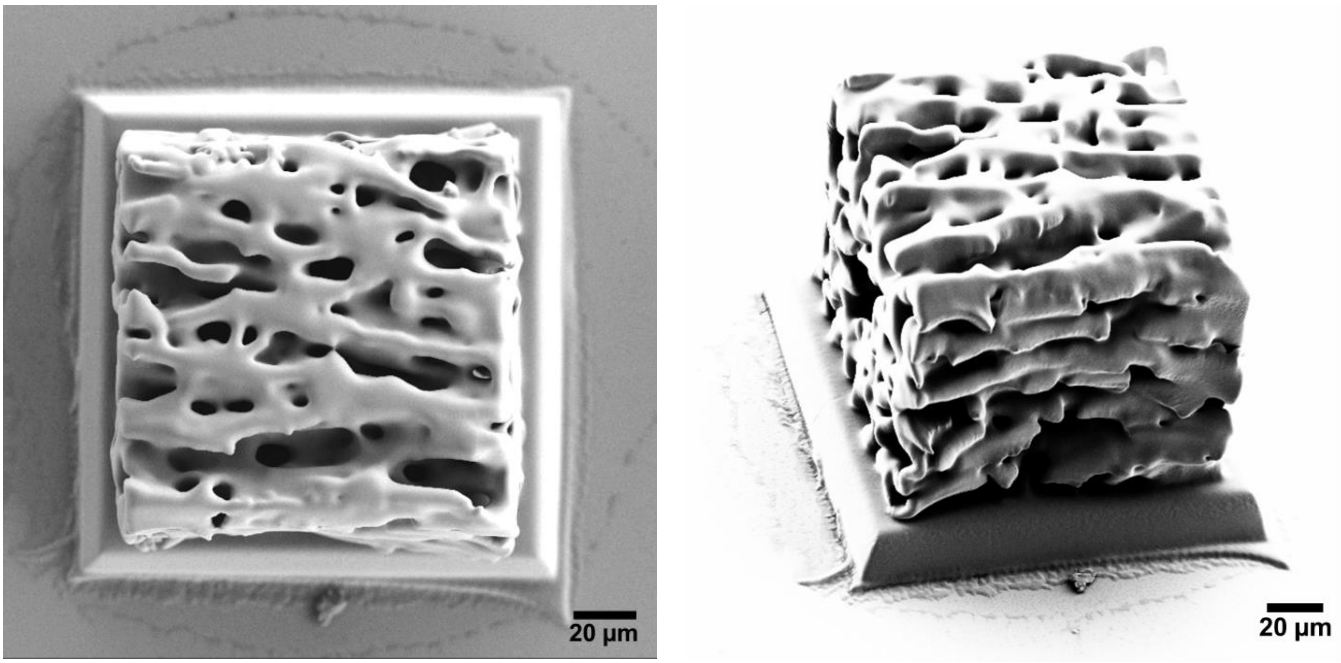

(**a**) (**b**)

Figure 3. Scanning electron micrographs of the porous scaffold structure. The porous structure itself is a cube with a side length of 133 µm, and is printed onto a solid base with a side length of 150 µm and a height of 15 µm. The structure was printed in the IP-PDMS resin on a plasma treated ITO-coated fused silica substrate using the 25×/0.80 microscope objective. (**a**) Top view. (**b**) Tilted view (45°).

3.2. High-Resolution Structures

Among all the existing 3D printing technologies, 2PP DLW is well recognized as providing the highest resolution. Consequently, 2PP enables the fabrication of intricate microscale structures with numerous very fine details.

Micropatterns can be employed to change the characteristics of a surface, for example its optical or wetting properties. Flat and high resolution micropatterns have been also previously exploited, e.g., control cell locomotion for migratory cells [45] or to reduce bacteria transference off contaminated surfaces [46]. However, the micropatterns employed in these examples were produced through several cleanroom fabrication steps, and therefore DLW would be an interesting alternative. We chose a mandala pattern (Figure 4) to emphasize the high resolution of 2PP for fabricating flat structures. The mandala is a complex abstract design with a semi-circular footprint, and it includes numerous small details, i.e., curved lines and small dots with critical dimension < 500 nm. The thickness of the mandala pattern is only 2 µm and is the same for the entire structure, which is why the mandala is considered a 2.5D structure.

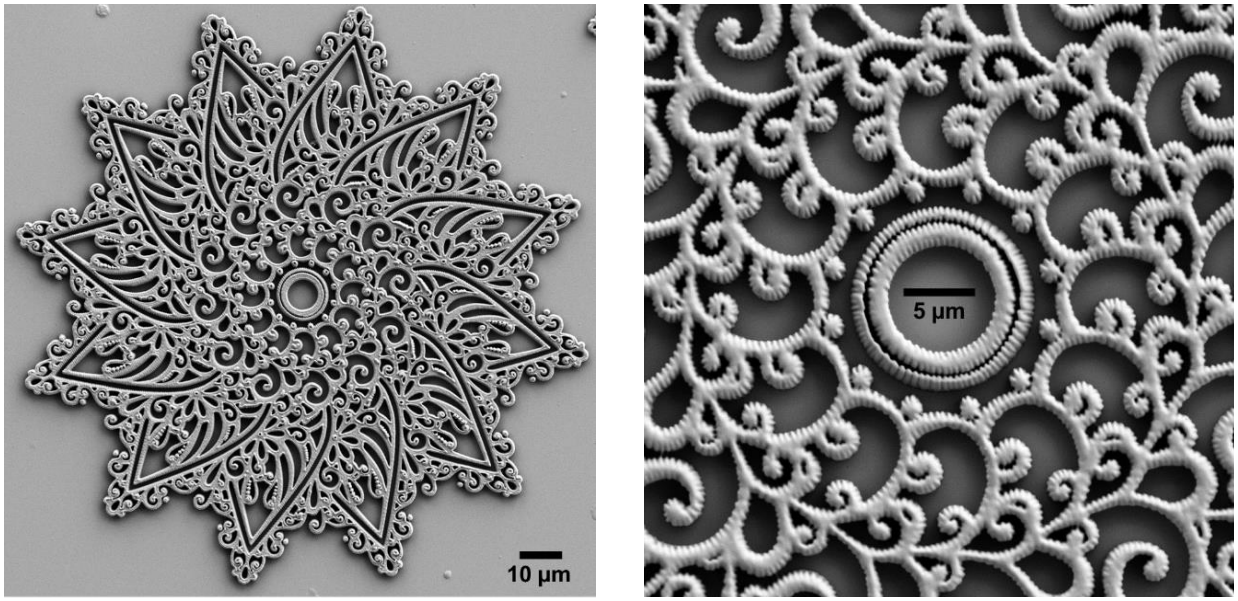

(**a**) (**b**)

Figure 4. Scanning electron micrographs of a mandala structure imaged using different magnifications. The entire structure has a diameter of 140 µm, a thickness of 2 µm, and features individual lines and dots with widths below 500 nm. The structure was printed in the IP-L 780 resin on a 170 µm thick borosilicate glass coverslip substrate using the 63×/1.40 microscope objective. (**a**) Full structure overview. (**b**) Enlarged central area.

Bioinspired micropatterns featuring conical micropillars with a height of 4–15 µm have been shown to modulate cell behaviors [47]. The pyramidal shape we chose is also very similar to that of microneedles, which typically have a height of several hundreds of micrometers, and are widely explored for painless drug administration [48]. We chose a pyramid architecture with a guarding sphynx assembly (Figure 5) to emphasize the high resolution of 2PP for tall structures. The pyramid includes numerous small details, whereas the sphynx has a rather smooth outer surface. Both the pyramid and the sphynx are truly 3D structures. From the optical profiler recordings, the measured height of the pyramid structure is 107 µm at its tip, and the sphynx's head is 51 µm tall. These values are in excellent agreement with the 3D design, where the pyramid has a height of 107 µm and the sphynx has a height of 53 µm.

3.3. Macroscale Structure

3D printing of macroscale structures has potential applications in for example optics, particularly for producing small lenses and other diffractive optical elements [49]. Unlike the other structures shown above, the fabricated Yggdrasil structure (Figure 6) has a size of 560 µm × 435 µm, which makes it visible on the substrate with the naked eye.

Although Nanoscribe recommends the use of AZ resins together with the 20×/0.50 microscope objective, it is nevertheless possible to use IP resins as well, as demonstrated here with IP-L 780 as example. However, the use of IP-L 780 for macroscale printing is not optimal. This is particularly obvious when looking at the fabrication parameters shown in Section 4, Table 2, in particular the extremely low scan speed employed for producing this structure, as opposed to the parameters employed when using the 63×/1.40 microscope objective for printing in IP-L 780.

3.4. Material Properties

Figure 7 shows representative XPS spectra and the corresponding analysis results for structures fabricated by 2PP DLW of IP-PDMS, as well as the acrylic IP-L 780 resin. As the resins employed in this study are proprietary commercial formulations, the information available about their composition and chemical properties is rather limited. 3D printing

of IP-PDMS results in polysiloxane structures containing carbon, hydrogen, oxygen, and silicon, whereas both IP-L 780 and IP-Dip contain hydrocarbon acrylates as polymer precursor, and thus result in polyacrylates that contain only carbon, hydrogen, and oxygen. Besides the polymer precursor, the commercial resin formulation contains a suitable solvent, as well as a two-photon photoinitiator. While the exact formulation of the IP-series resins is not public, various photoinitiators for two-photon polymerization are discussed in detail elsewhere [50].

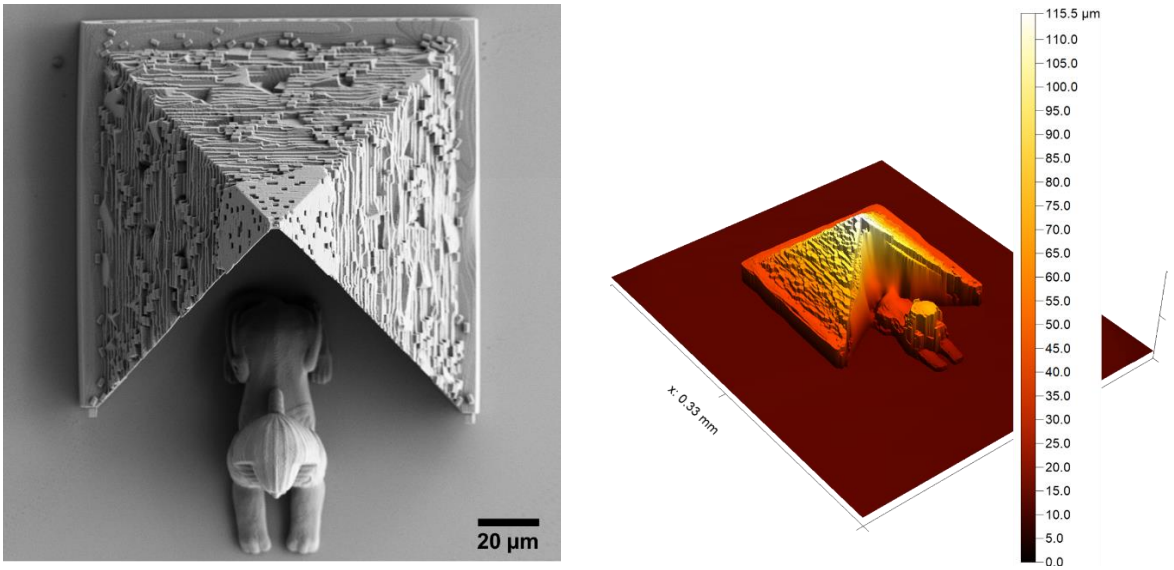

(**a**) (**b**)

Figure 5. Pyramid with guarding sphynx structure. The pyramid has a base length of 139 µm and a height of 107 µm, whereas the sphynx has a height of 51 µm. The structure was printed in the IP-Dip resin on a fused silica substrate using the 63×/1.40 microscope objective. (**a**) Scanning electron micrograph. (**b**) Natural proportion image generated using optical profilometry.

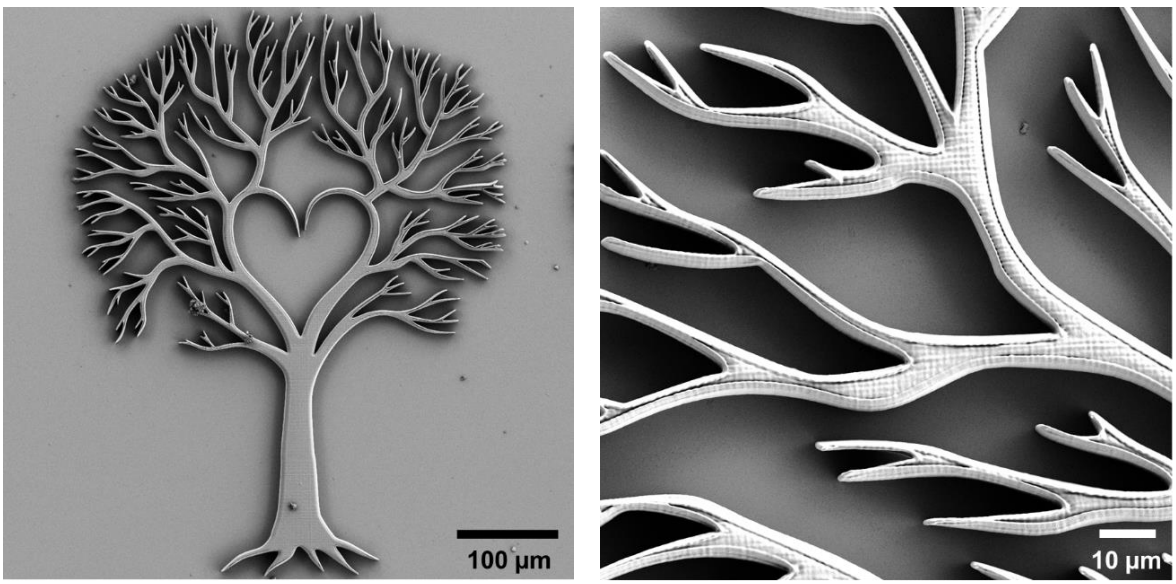

(**a**) (**b**)

Figure 6. Scanning electron micrographs of the Yggdrasil structure imaged using different magnifications. The entire Scheme 560 µm × 435 µm and a thickness of 2 µm. The structure was printed in the IP-L 780 resin on a 170 µm thick borosilicate glass coverslip substrate using the 20×/0.50 microscope objective. (**a**) Full structure overview. (**b**) Enlarged area from top left region of the structure.

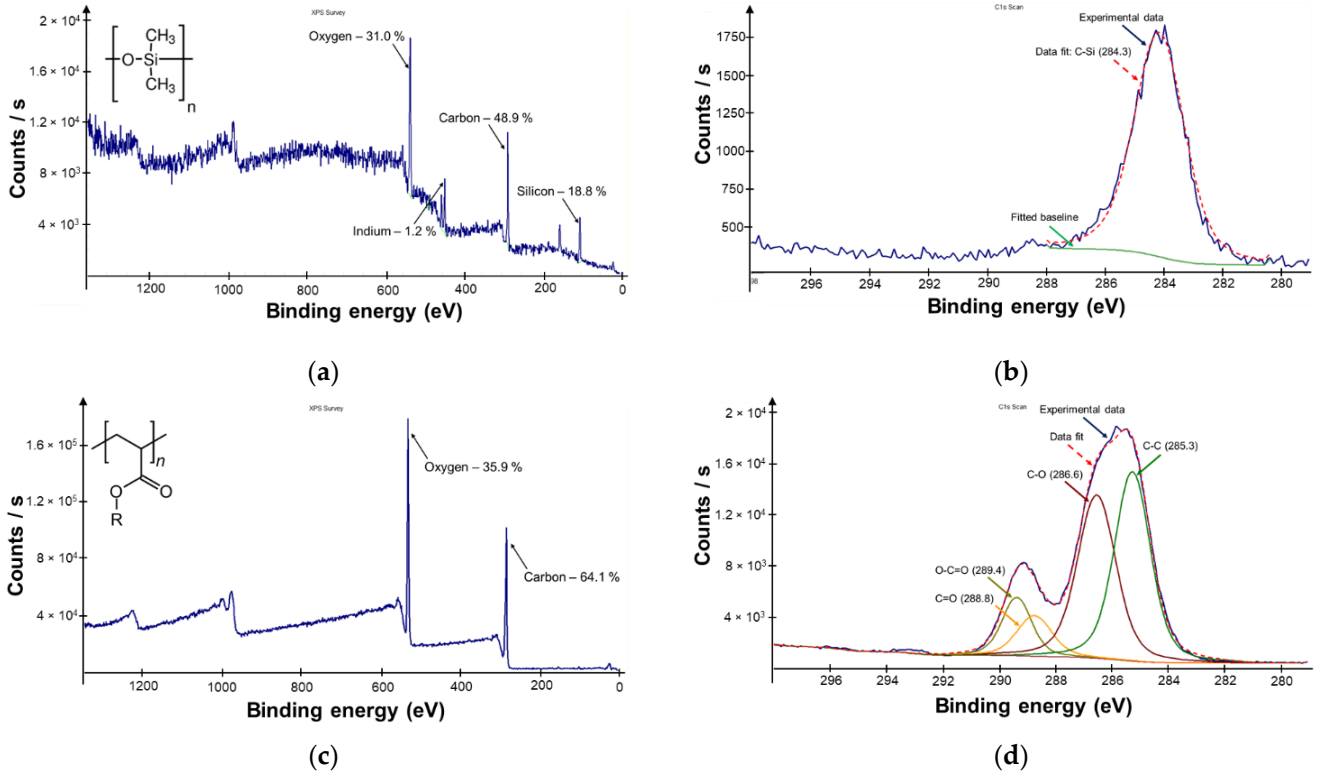

Figure 7. X-ray photoelectron spectroscopy (XPS) analysis of flat 3D printed structures. (**a**,**b**) IP-PDMS. (**c**,**d**) IP-L 780. (**a**,**c**) Survey spectra showing the quantified elements and their relative abundance. Insert shows the chemical structure of the polymer. (**b**,**d**) High-resolution C1s spectra with peak deconvolution showing the types of chemical bonds identified.

In order to gather more information about the surface chemistry of the polymers after 2PP, XPS analysis was performed on flat structures fabricated using the three resins in the same manner as their microstructured counterparts.

As expected, the XPS survey spectrum for IP-PDMS confirms the presence of oxygen, carbon, and silicon. Additionally, small amounts of indium are identified, which can be attributed to the ITO coating present on the substrate. In the case of IP-L 780, only carbon and oxygen are identified. As XPS cannot detect hydrogen, this element is not present in the survey spectra shown. The results obtained using IP-L 780 and IP-Dip are extremely similar (data not shown). To further validate our understanding of the chemical composition of the two polymers, we performed a more detailed analysis of the corresponding high-resolution C1s XPS spectra. For IP-PDMS, the spectrum shows a single peak centered at 284.3 eV, corresponding to the C-Si σ bond. For the acrylic polymer, peak deconvolution confirms the presence of C-C and C-O σ bonds, as well as C=O bonds and O–C=O groups, with binding energies similar to those encountered in the literature for similar structures [51].

4. Discussion

Each microscope objective has a characteristic field of view. When printing on the Nanoscribe Photonic Professional GT+, each microscope objective also has a characteristic maximum effective writing field, which is a circle inscribed within the maximum field of view. Figure 8a shows the maximum effective writing field corresponding to our three microscope objectives as concentric circles. Outside the maximum effective writing field, aberrations can significantly impact print quality. In order to fabricate structures larger than the maximum writing field, stitching of multiple print areas is required.

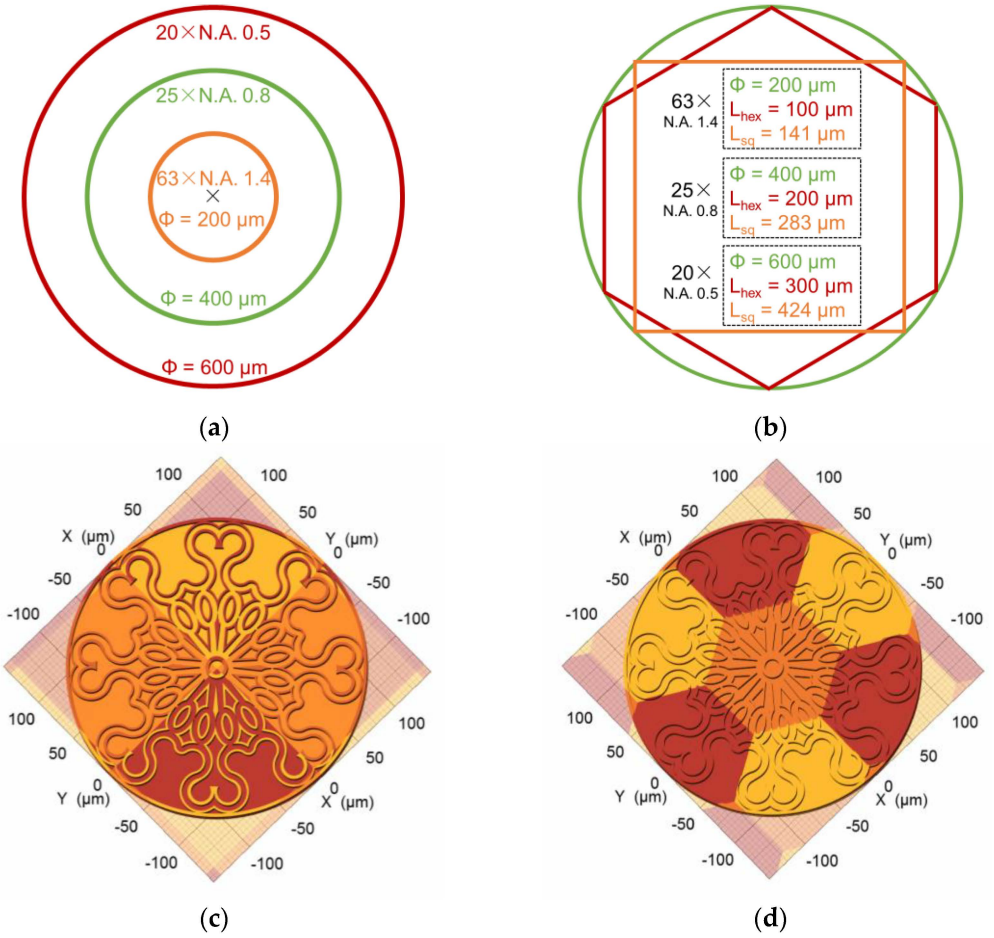

Figure 8. (**a**) The maximum effective writing field corresponding to our three microscope objectives, shown as concentric circles. (**b**) Geometry and size of the maximum effective writing field, as well as the corresponding largest inscribed square and hexagon, where L is the side length, for our three microscope objectives. (**c**,**d**) Structure splitting into printing blocks with a (**c**) square and (**d**) hexagonal shape, using the rosette window cookie master and the 63× objective as example.

The DeScribe software allows for automatic splitting of a structure into blocks, which can be either square or hexagonal. The geometry and size of the maximum effective writing field, as well as the corresponding largest inscribed square and hexagon, for our three microscope objectives is shown in Figure 8b. Figure 8c,d show a large structure split into several printing blocks with a square and hexagonal shape, respectively.

When it comes to achieving the highest resolution for 2PP 3D printing, the 63×/1.40 microscope objective is an obvious choice. However, there are two options regarding the configuration for printing, as on the Nanoscribe systems it is possible to print "upwards" or "downwards" with respect to the Z-axis. The two corresponding configurations are denoted as "immersion" and "DiLL", respectively. As shown in Figure 9a, in immersion configuration, the resin is placed on the top of an ultrathin glass substrate. When using the 63×/1.40 microscope objective, a drop of immersion oil with a refractive index matching that of the substrate is first applied onto the microscope objective. In this case, the laser beam coming through the microscope objective is focused through the oil and the substrate into the resin. Printing starts on the interface between the substrate and the resin and proceeds upwards. On the 63×/1.40 objective, the structure height is limited by the working distance to 190 µm. However, aberrations increase with structure height, especially when the beam is focused through a thick layer of crosslinked resin [16]. On the other hand, as shown in Figure 9b, in DiLL configuration, also known as dip-in, the microscope objective is directly immersed into the resin, which is placed on the bottom of the substrate. The resin acts as both polymer precursor and immersion medium. In

this case, the laser beam coming through the microscope objective is focused only through the liquid resin. Printing starts on the interface between the resin and the substrate and proceeds downwards. Furthermore, the aberrations are constant, regardless of the height and geometry of the structure. On the 63×/1.40 objective, the structure height can go beyond 300 µm in DiLL mode, according to the producer's specifications.

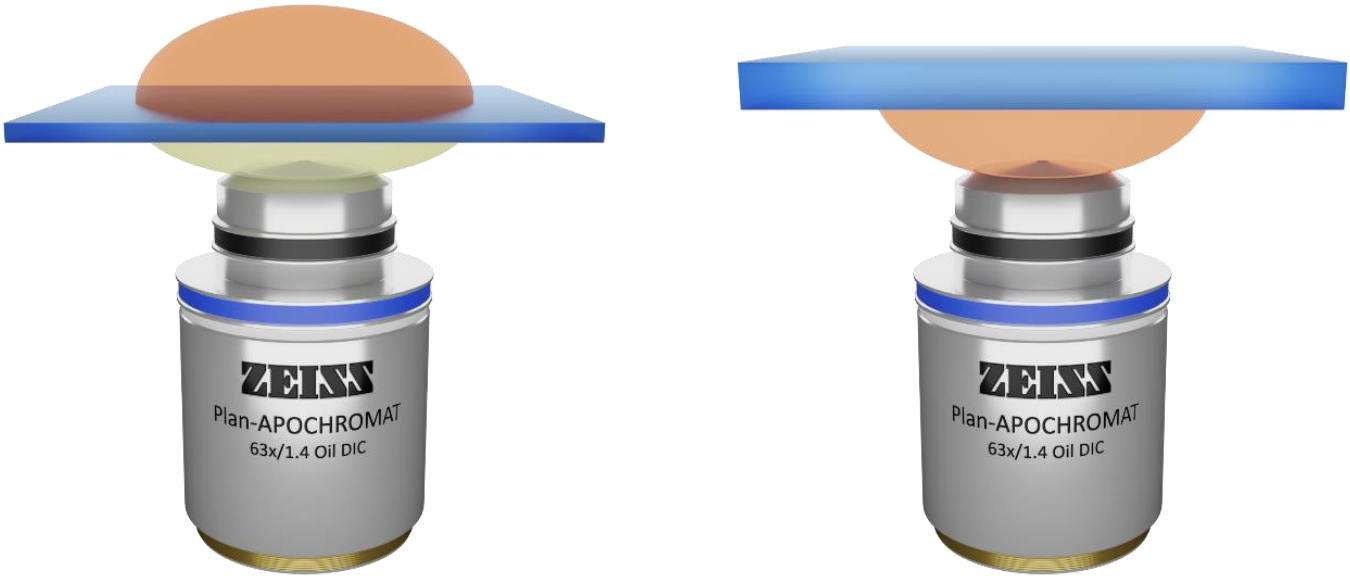

(**a**) (**b**)

Figure 9. Schematic representation of the setup for printing in (**a**) oil immersion and (**b**) DiLL configuration.

High resolution printing can be achieved using the 63×/1.40 microscope objective in either oil immersion or DiLL mode. However, the two configurations have characteristic advantages and disadvantages, depending on the target structure. For relatively thin and flat structures, small features can be more challenging to fabricate in DiLL mode, as shown in Figure 10a,b. For the chosen mandala structure, the smallest features are not properly developed for the DiLL print, as opposed to the oil immersion print. On the other hand, tall structures are rather challenging to achieve in oil immersion mode, as shown in Figure 10c,d. The tip of the pyramid printed in the oil immersion configuration is deformed and the front side walls are collapsed, as opposed to the DiLL print, where the structure is intact.

Large objects can be printed by stitching multiple small print areas or by using a microscope objective with a rather large effective writing field. However, simply taking a larger object and printing it by stitching multiple print areas is likely to result in artefacts, as it can be seen in Figure 11. In order to achieve a high quality print by stitching multiple blocks, it is often necessary to optimize, e.g., the block shape, writing order, and shear angle. Instead, for printing large arrays of small structures, it is often sufficient to split the array in a reasonable manner, i.e., by ensuring that individual structures are contained in each printing block. We have previously demonstrated error-free fabrication of a 1 × 1 mm^2 array of smooth muscle cell-mimicking structures [16]. The best solution for fabricating macroscale objects therefore depends on the necessary resolution and on how dedicated a user might be to optimizing the printing process. Stitching-free 2PP 3D printing of millimeter-sized optical components was recently demonstrated using a 10×/0.30 microscope objective with a writing field of 1 mm used in DiLL mode, together with the IP-Visio resin [49]. When sub-micrometer resolution is not crucial, but any stitching might interfere with the structure's function, selecting a microscope objective with a low numerical aperture, but a large effective writing field, is highly beneficial. Instead, if critical dimensions of

100–200 nm are essential for the macroscale structure, optimization of the stitching of small blocks printed using the 63×/1.40 microscope objective is likely necessary.

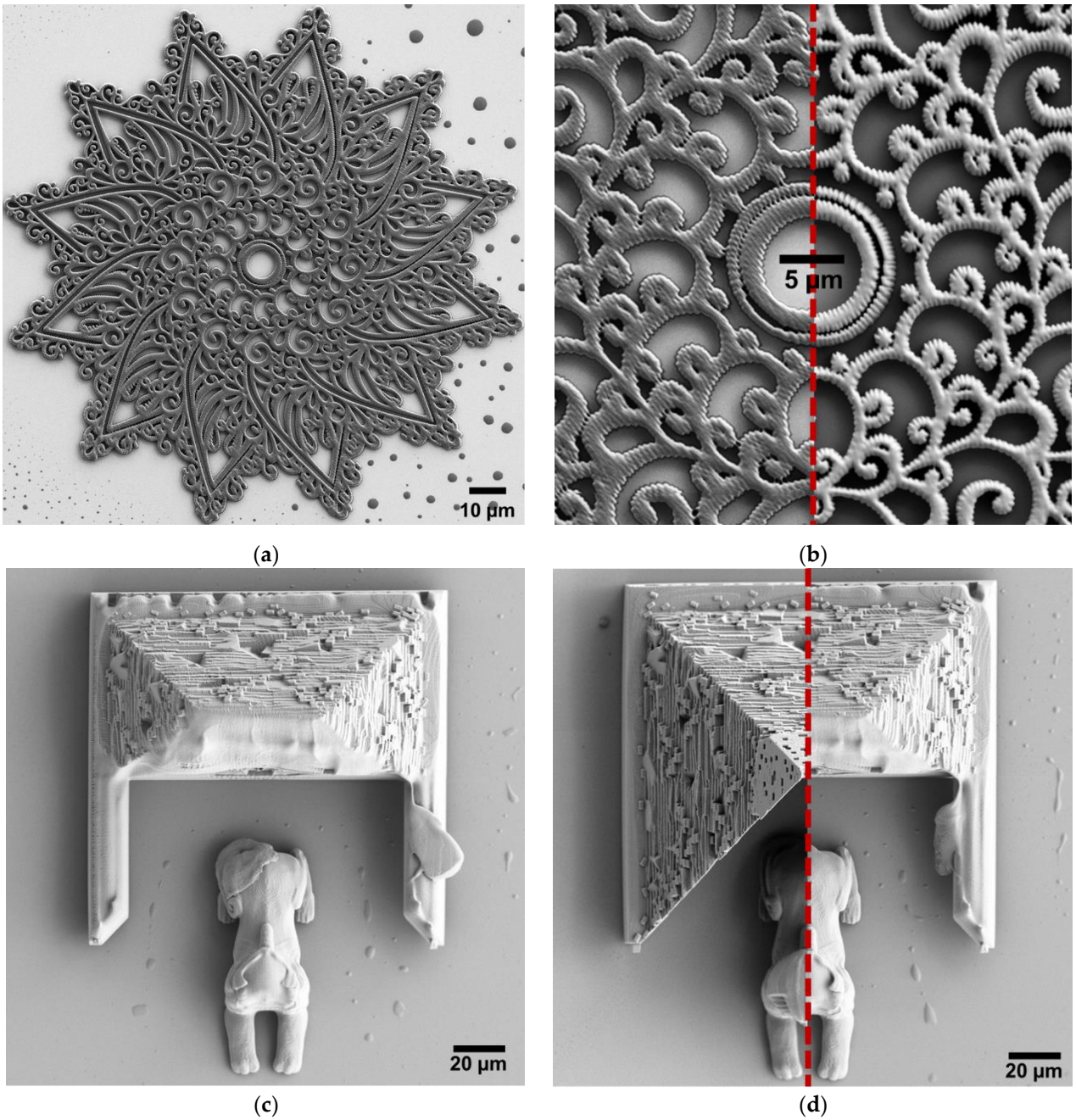

(**a**) (**b**) (**c**) (**d**)

Figure 10. (**a**,**b**) Scanning electron micrographs of the mandala structure imaged using different magnifications. (**a**) Structure printed in DiLL mode in the IP-Dip resin on a 0.7 mm thick fused silica substrate using the 63×/1.40 microscope objective. (**b**) Composite image showing the center of the mandala structure fabricated using (left) DiLL/IP-Dip and (right) oil immersion/IP-L 780. (**c**,**d**) Scanning electron micrographs of the pyramid with guarding sphynx structure. (**c**) Structure printed in DiLL mode in the IP-Dip resin on a 0.7 mm thick fused silica substrate using the 63×/1.40 microscope objective. (**d**) Composite image showing the structure fabricated using (left) DiLL/IP-Dip and (right) oil immersion/IP-L 780.

Parameter optimization is always one of the necessary steps to achieve the best possible printed structures on the Nanoscribe. However, given the number of different parameters that can be varied, having a reasonable starting point is a crucial part of speeding up the optimization process. Consequently, based on our experience, and as

supported by the results shown above, we compiled in Table 1 a quick guide for selecting the microscope objective, configuration, substrate, resin, and slicing and hatching distances on the Nanoscribe, depending on the type of target microstructure. For every specific target structure, the slicing and hatching distances can be further optimized, together with other parameters, among which the laser power and scan speed are likely the most important. This part of the optimization is described rather well in the Nanoscribe guide provided with the equipment, and the preset parameters from the system can serve as starting point for the optimization, so we will not go into additional details, as the optimal parameters depend on individual structures and systems.

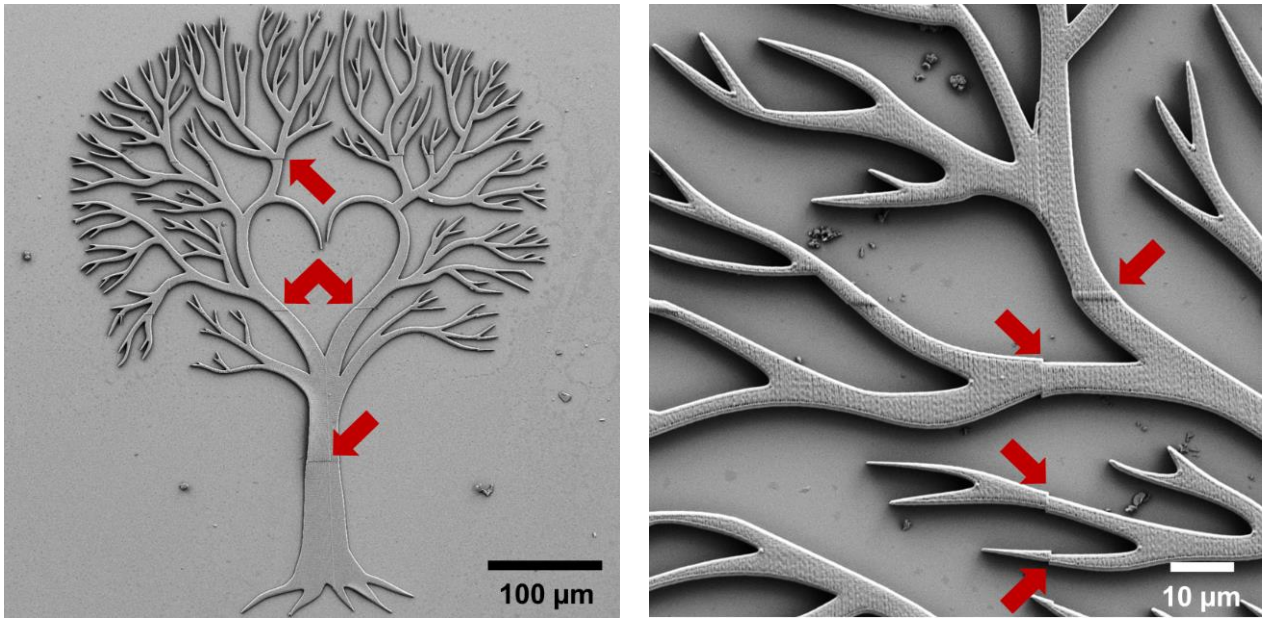

(**a**) (**b**)

Figure 11. Scanning electron micrographs of the Yggdrasil structure imaged using different magnifications. The entire structure has a length of 560 µm and a thickness of 6 µm. The structure was printed by stitching square blocks with a size of 140 × 140 µm^2 in the IP-L 780 resin on a 170 µm thick borosilicate glass coverslip substrate using the 63×/1.40 microscope objective. The red arrows point at small stitching errors. (**a**) Full structure overview. (**b**) Enlarged area from top left region of the structure.

5. Conclusions

Two-photon polymerization-based direct laser writing is an excellent technological solution for the fabrication of micro-, meso-, and even macroscale structures with extremely fine features. However, the quality of the 3D printed structures depends on many different fabrication parameters, starting with the employed microscope objective, printing configuration, substrate, and resin. Additionally, other fabrication parameters, including the laser power and scan speed, as well as post-processing solutions, are likely to affect the final printed product. This paper discusses such parameters and demonstrates the fabrication of microscale soft structures, high-resolution 2.5D and 3D structures, and a macroscopic structure. Our results and discussion should be highly beneficial for scientists entering the research field of two-photon polymerization, particularly for new Nanoscribe users. Having a good starting point for the fabrication of various types of structures will speed up the optimization procedure, ultimately enabling researchers to produce structures with interesting and valuable applications.

Supplementary Materials: The following are available online at https://www.mdpi.com/article/10.3390/micro1020013/s1, Section S1: 3D design files (.STL), Section S2: Printing file preparation (.GWL), Figure S1: 3D renders of the designs employed for fabricating the structures shown in the main text, Table S1: Sizes defined in DeScribe for the various structures fabricated.

Author Contributions: Conceptualization, A.-I.B.; investigation, A.-I.B., N.d.C.I., A.D. and E.E.; resources, A.-I.B. and R.T.; writing—original draft preparation, A.-I.B.; writing—review and editing, N.d.C.I., A.D., A.E.W., E.E. and R.T.; visualization, A.-I.B., N.d.C.I., A.D. and A.E.W.; supervision, A.-I.B. and R.T.; and funding acquisition, A.-I.B. All authors have read and agreed to the published version of the manuscript.

Funding: This research was funded by VILLUM FONDEN, grant numbers 34424 and 00022918, and Novo Nordisk Foundation, grant number NNF16OC0021948. The APC was funded by grant 34424.

Data Availability Statement: Raw data is available from the authors upon reasonable request.

Acknowledgments: The authors would like to acknowledge the DTU Nanolab staff for technical support and equipment trainings.

Conflicts of Interest: The authors declare no conflict of interest. The funders had no role in the design of the study; in the collection, analyses, or interpretation of data; in the writing of the manuscript, or in the decision to publish the results.

References

1. Gebhardt, A. *Understanding Additive Manufacturing*; Carl Hanser Verlag GmbH & Co. KG: Munich, Germany, 2011; ISBN 978-3-446-43162-1.
2. Nadagouda, M.N.; Rastogi, V.; Ginn, M. A review on 3D printing techniques for medical applications. *Curr. Opin. Chem. Eng.* **2020**, *28*, 152–157. [CrossRef]
3. El-Sayegh, S.; Romdhane, L.; Manjikian, S. A critical review of 3D printing in construction: Benefits, challenges, and risks. *Arch. Civ. Mech. Eng.* **2020**, *20*, 3. [CrossRef]
4. Mantihal, S.; Kobun, R.; Lee, B.B. 3D food printing of as the new way of preparing food: A review. *Int. J. Gastron. Food Sci.* **2020**, *22*, 100260. [CrossRef]
5. Kawata, S.; Sun, H.B.; Tanaka, T.; Takada, K. Finer features for functional microdevices. *Nature* **2001**, *412*, 697–698. [CrossRef] [PubMed]
6. Fischer, J.; Wegener, M. Three-dimensional optical laser lithography beyond the diffraction limit. *Laser Photonics Rev.* **2013**, *7*, 22–44. [CrossRef]
7. Göppert-Mayer, M. Über Elementarakte mit zwei Quantensprüngen. *Ann. Phys.* **1931**, *401*, 273–294. [CrossRef]
8. Kaiser, W.; Garrett, C.G.B. Two-photon excitation in CaF2: Eu2+. *Phys. Rev. Lett.* **1961**, *7*, 229–231. [CrossRef]
9. Baldacchini, T. *Three-Dimensional Microfabrication Using Two-Photon Polymerization: Fundamentas, Technology and Applications*; Elsevier: Waltham, MA, USA, 2016; ISBN 978-0-323-35321-2.
10. Zhou, X.; Hou, Y.; Lin, J. A review on the processing accuracy of two-photon polymerization. *AIP Adv.* **2015**, *5*, 30701. [CrossRef]
11. Maruo, S.; Nakamura, O.; Kawata, S. Three-dimensional microfabrication with two-photon-absorbed photopolymerization. *Opt. Lett.* **1997**, *22*, 132. [CrossRef]
12. Engay, E.; Bunea, A.-I.; Chouliara, M.; Bañas, A.; Glückstad, J. Natural convection induced by an optically fabricated and actuated microtool with a thermoplasmonic disk. *Opt. Lett.* **2018**, *43*, 3870–3873. [CrossRef]
13. Bunea, A.; Martella, D.; Nocentini, S.; Parmeggiani, C.; Taboryski, R.; Wiersma, D.S. Light-Powered Microrobots: Challenges and Opportunities for Hard and Soft Responsive Microswimmers. *Adv. Intell. Syst.* **2021**, *3*, 2000256. [CrossRef]
14. Kim, J.A.; Wales, D.J.; Thompson, A.J.; Yang, G. Fiber-Optic SERS Probes Fabricated Using Two-Photon Polymerization For Rapid Detection of Bacteria. *Adv. Opt. Mater.* **2020**, *8*, 1901934. [CrossRef]
15. Park, S.; Nguyen, D.V.; Kang, L. Immobilized nanoneedle-like structures for intracellular delivery, biosensing and cellular surgery. *Nanomedicine* **2021**, *16*, 335–349. [CrossRef] [PubMed]
16. Sabaté Rovira, D.; Nielsen, H.M.; Taboryski, R.; Bunea, A.I. Additive manufacturing of polymeric scaffolds for biomimetic cell membrane engineering. *Mater. Des.* **2021**, *201*, 109486. [CrossRef]
17. Bunea, A.I.; Jakobsen, M.H.; Engay, E.; Bañas, A.R.; Glückstad, J. Optimization of 3D-printed microstructures for investigating the properties of the mucus biobarrier. *Micro Nano Eng.* **2019**, *2*, 41–47. [CrossRef]
18. Cumpston, B.H.; Ananthavel, S.P.; Barlow, S.; Dyer, D.L.; Ehrlich, J.E.; Erskine, L.L.; Heikal, A.A.; Kuebler, S.M.; Lee, I.Y.S.; McCord-Maughon, D.; et al. Two-photon polymerization initiators for three-dimensional optical data storage and microfabrication. *Nature* **1999**, *398*, 51–54. [CrossRef]
19. Li, J.; Fejes, P.; Lorenser, D.; Quirk, B.C.; Noble, P.B.; Kirk, R.W.; Orth, A.; Wood, F.M.; Gibson, B.C.; Sampson, D.D.; et al. Two-photon polymerisation 3D printed freeform micro-optics for optical coherence tomography fibre probes. *Sci. Rep.* **2018**, *8*, 14789. [CrossRef] [PubMed]
20. Weber, K.; Werdehausen, D.; König, P.; Thiele, S.; Schmid, M.; Decker, M.; De Oliveira, P.W.; Herkommer, A.; Giessen, H. Tailored nanocomposites for 3D printed micro-optics. *Opt. Mater. Express* **2020**, *10*, 2345. [CrossRef]
21. Wetzel, A.E.; del Iniesta, N.C.; Engay, E.; Mandsberg, N.K.; Dinesen, C.S.; Hanif, B.R.; Berg-Sørensen, K.; Bunea, A.-I.; Taboryski, R. Bioinspired Microstructured Polymer Surfaces with Antireflective Properties. *Nanomaterials* **2021**, *11*, 2298. [CrossRef]

22. Soukoulis, C.M.; Wegener, M. Past achievements and future challenges in the development of three-dimensional photonic metamaterials. *Nat. Photonics* **2011**, *5*, 523–530. [CrossRef]
23. Von Freymann, G.; Ledermann, A.; Thiel, M.; Staude, I.; Essig, S.; Busch, K.; Wegener, M. Three-Dimensional Nanostructures for Photonics. *Adv. Funct. Mater.* **2010**, *20*, 1038–1052. [CrossRef]
24. Bückmann, T.; Stenger, N.; Kadic, M.; Kaschke, J.; Frölich, A.; Kennerknecht, T.; Eberl, C.; Thiel, M.; Wegener, M. Tailored 3D Mechanical Metamaterials Made by Dip-in Direct-Laser-Writing Optical Lithography. *Adv. Mater.* **2012**, *24*, 2710–2714. [CrossRef]
25. Tudor, A.; Delaney, C.; Zhang, H.; Thompson, A.J.; Curto, V.F.; Yang, G.Z.; Higgins, M.J.; Diamond, D.; Florea, L. Fabrication of soft, stimulus-responsive structures with sub-micron resolution via two-photon polymerization of poly(ionic liquid)s. *Mater. Today* **2018**, *21*, 807–816. [CrossRef]
26. Del Pozo, M.; Delaney, C.; Bastiaansen, C.W.M.; Diamond, D.; Schenning, A.P.H.J.; Florea, L. Direct laser writing of four-dimensional structural color microactuators using a photonic photoresist. *ACS Nano* **2020**, *14*, 9832–9839. [CrossRef]
27. Nocentini, S.; Martella, D.; Parmeggiani, C.; Wiersma, D.S. 3D printed photoresponsive materials for photonics. *Adv. Opt. Mater.* **2019**, *7*, 1900156. [CrossRef]
28. Dai, G.; Hu, X.; Hering, J.; Eifler, M.; Seewig, J.; Freymann, G. von Define and measure the dimensional accuracy of two-photon laser lithography based on its instrument transfer function. *J. Phys. Photonics* **2021**, *3*, 034002. [CrossRef]
29. Oakdale, J.S.; Ye, J.; Smith, W.L.; Biener, J. Post-print UV curing method for improving the mechanical properties of prototypes derived from two-photon lithography. *Opt. Express* **2016**, *24*, 27077. [CrossRef]
30. Bauer, J.; Guell Izard, A.; Zhang, Y.; Baldacchini, T.; Valdevit, L. Thermal post-curing as an efficient strategy to eliminate process parameter sensitivity in the mechanical properties of two-photon polymerized materials. *Opt. Express* **2020**, *28*, 20362. [CrossRef] [PubMed]
31. Jiang, L.J.; Zhou, Y.S.; Xiong, W.; Gao, Y.; Huang, X.; Jiang, L.; Baldacchini, T.; Silvain, J.-F.; Lu, Y.F. Two-photon polymerization: Investigation of chemical and mechanical properties of resins using Raman microspectroscopy. *Opt. Lett.* **2014**, *39*, 3034. [CrossRef] [PubMed]
32. Bougdid, Y.; Sekkat, Z. Voxels Optimization in 3D Laser Nanoprinting. *Sci. Rep.* **2020**, *10*, 10409. [CrossRef] [PubMed]
33. Gernhardt, M.; Blasco, E.; Hippler, M.; Blinco, J.; Bastmeyer, M.; Wegener, M.; Frisch, H.; Barner-Kowollik, C. Tailoring the Mechanical Properties of 3D Microstructures Using Visible Light Post-Manufacturing. *Adv. Mater.* **2019**, *31*, 1901269. [CrossRef]
34. Purtov, J.; Verch, A.; Rogin, P.; Hensel, R. Improved development procedure to enhance the stability of microstructures created by two-photon polymerization. *Microelectron. Eng.* **2018**, *194*, 45–50. [CrossRef]
35. Seniutinas, G.; Weber, A.; Padeste, C.; Sakellari, I.; Farsari, M.; David, C. Beyond 100 nm resolution in 3D laser lithography—Post processing solutions. *Microelectron. Eng.* **2018**, *191*, 25–31. [CrossRef]
36. Chidambaram, N.; Kirchner, R.; Fallica, R.; Yu, L.; Altana, M.; Schift, H. Selective Surface Smoothening of Polymer Microlenses by Depth Confined Softening. *Adv. Mater. Technol.* **2017**, *2*, 1700018. [CrossRef]
37. Kirchner, R.; Schift, H. Thermal reflow of polymers for innovative and smart 3D structures: A review. *Mater. Sci. Semicond. Process.* **2019**, *92*, 58–72. [CrossRef]
38. Nečas, D.; Klapetek, P. Gwyddion: An open-source software for SPM data analysis. *Cent. Eur. J. Phys.* **2012**, *10*, 181–188. [CrossRef]
39. Tanzi, S.; Ostergaard, P.F.; Matteucci, M.; Christiansen, T.L.; Cech, J.; Marie, R.; Taboryski, R. Fabrication of combined-scale nano- and microfluidic polymer systems using a multilevel dry etching, electroplating and molding process. *J. Micromech. Microeng.* **2012**, *22*, 115008. [CrossRef]
40. Murthy, S.; Matschuk, M.; Huang, Q.; Mandsberg, N.K.; Feidenhans'l, N.A.; Johansen, P.; Christensen, L.; Pranov, H.; Kofod, G.; Pedersen, H.C.; et al. Fabrication of Nanostructures by Roll-to-Roll Extrusion Coating. *Adv. Eng. Mater.* **2016**, *18*, 484–489. [CrossRef]
41. Murthy, S.; Pranov, H.; Feidenhans'L, N.A.; Madsen, J.S.; Hansen, P.E.; Pedersen, H.C.; Taboryski, R. Plasmonic color metasurfaces fabricated by a high speed roll-to-roll method. *Nanoscale* **2017**, *9*, 14280–14287. [CrossRef]
42. Okulova, N.; Johansen, P.; Christensen, L.; Taboryski, R. Effect of Structure Hierarchy for Superhydrophobic Polymer Surfaces Studied by Droplet Evaporation. *Nanomaterials* **2018**, *8*, 831. [CrossRef]
43. Lemma, E.D.; Rizzi, F.; Dattoma, T.; Spagnolo, B.; Sileo, L.; Qualtieri, A.; De Vittorio, M.; Pisanello, F. Mechanical Properties Tunability of Three-Dimensional Polymeric Structures in Two-Photon Lithography. *IEEE Trans. Nanotechnol.* **2017**, *16*, 23–31. [CrossRef]
44. Guimarães, C.F.; Gasperini, L.; Marques, A.P.; Reis, R.L. The stiffness of living tissues and its implications for tissue engineering. *Nat. Rev. Mater.* **2020**, *5*, 351–370. [CrossRef]
45. Yoon, S.H.; Kim, Y.K.; Han, E.D.; Seo, Y.H.; Kim, B.H.; Mofrad, M.R.K. Passive control of cell locomotion using micropatterns: The effect of micropattern geometry on the migratory behavior of adherent cells. *Lab. Chip* **2012**, *12*, 2391–2402. [CrossRef] [PubMed]
46. Xu, B.; Wei, Q.; Mettetal, M.R.; Han, J.; Rau, L.; Tie, J.; May, R.M.; Pathe, E.T.; Reddy, S.T.; Sullivan, L.; et al. Surface micropattern reduces colonization and medical device-associated infections. *J. Med. Microbiol.* **2017**, *66*, 1692–1698. [CrossRef] [PubMed]
47. Dai, J.; Kong, N.; Lu, Y.; Yuan, Y.; Wu, Q.; Shi, M.; Zhang, S.; Wu, Y.; Peng, W.; Huang, P.; et al. Bioinspired Conical Micropattern Modulates Cell Behaviors. *ACS Appl. Bio. Mater.* **2018**, *1*, 1416–1423. [CrossRef]
48. Prausnitz, M.R. Microneedles for transdermal drug delivery. *Adv. Drug Deliv. Rev.* **2004**, *56*, 581–587. [CrossRef]

49. Ristok, S.; Thiele, S.; Toulouse, A.; Herkommer, A.M.; Giessen, H. Stitching-free 3D printing of millimeter-sized highly transparent spherical and aspherical optical components. *Opt. Mater. Express* **2020**, *10*, 2370. [CrossRef]
50. Huang, Z.; Tsui, G.C.-P.; Deng, Y.; Tang, C.-Y. Two-photon polymerization nanolithography technology for fabrication of stimulus-responsive micro/nano-structures for biomedical applications. *Nanotechnol. Rev.* **2020**, *9*, 1118–1136. [CrossRef]
51. Goseki, R.; Hong, L.; Inutsuka, M.; Yokoyama, H.; Ito, K.; Ishizone, T. Synthesis and surface characterization of well-defined amphiphilic block copolymers composed of polydimethylsiloxane and poly[oligo(ethylene glycol) methacrylate]. *RSC Adv.* **2017**, *7*, 25199–25207. [CrossRef]